2019

Differential Spatial Gradients of Wheat Streak Mosaic Virus into Winter Wheat from a Central Mite-Virus Source

Abby R. Stilwell
USDA APHIS

Donald Rundquist
University of Nebraska - Lincoln, drundquist1@unl.edu

David B. Marx
University of Nebraska-Lincoln, david.marx@unl.edu

Gary L. Hein
University of Nebraska - Lincoln, ghein1@unl.edu

Plant Disease • 2019 • 103:338-344 • https://doi.org/10.1094/PDIS-01-18-0025-RE

Differential Spatial Gradients of Wheat Streak Mosaic Virus into Winter Wheat from a Central Mite-Virus Source

Abby R. Stilwell, U.S. Department of Agriculture, Animal and Plant Health Inspection Service, Plant Protection and Quarantine, Raleigh, NC; **Donald C. Rundquist,** School of Natural Resources, University of Nebraska–Lincoln; **David B. Marx,** Department of Statistics, University of Nebraska–Lincoln; and **Gary L. Hein,**† Plant Health Program, University of Nebraska–Lincoln

Abstract

The wheat curl mite (WCM), *Aceria tosichella* Keifer, transmits three potentially devastating viruses to winter wheat. An increased understanding of mite movement and subsequent virus spread through the landscape is necessary to estimate the risk of epidemics by the virus in winter wheat. Owing to the small size of WCMs, their dispersal via wind is hard to monitor; however, the viruses they transmit produce symptoms that can be detected with remote sensing. The objective of this study was to characterize the spatial dispersal of the virus from a central mite-virus source. Virus infection gradients were measured spatially by using aerial remote sensing, ground measurements, geostatistics, and a geographic information system between 2006 and 2009. The red edge position vegetation index as measured via aerial imagery was significantly correlated with in-field biophysical measurements. The occurrence of virus symptoms extended differentially in all directions from mite-virus source plots, and predictions from cokriging revealed an oval pattern surrounding the source but displaced to the southeast. The variable dispersal in different directions appeared to be influenced by the mite source density and wind direction and speed, but temperature also seemed likely to have affected mite spread. The spatial spread revealed in this study may be used to estimate the potential sphere of influence of mite-infested volunteer wheat in production fields. These risk parameter estimates require further validation, but they may potentially aid growers in making better virus management decisions regarding differential virus spread potential away from a central source.

The wheat curl mite (WCM), *Aceria tosichella* Keifer, is a small eriophyid mite (approximately 250 μm in length) that is widely distributed in North America (Oldfield 1970). The mite transmits three viruses to wheat: wheat streak mosaic virus (WSMV), High Plains wheat mosaic virus (Seifers et al. 1997), and Triticum mosaic virus (Seifers et al. 2008). Although all three viruses are commonly found, WSMV is the predominant mite-vectored virus in winter wheat in the Great Plains (Burrows et al. 2009; Byamukama et al. 2013). This disease complex is potentially the most devastating disease of winter wheat in the central Great Plains, and infections in individual fields often result in complete crop failure (Wegulo et al. 2008).

Mites can only survive about 1 to 2 days off living plants when temperatures are above about 25°C (Wosula et al. 2015); therefore, they must exploit an alternate host to bridge the gap between wheat harvest and emergence of the newly planted wheat in the fall (Connin 1956). In the central Great Plains, the most important bridge host utilized by mites is volunteer wheat that results when preharvest hail storms shatter grain onto the ground, enabling it to germinate and grow rapidly (Staples and Allington 1956; Wegulo et al. 2008). As wheat approaches maturity and harvest, mite populations are high, and volunteer wheat emerging at this time is quickly infested with mites as they disperse from maturing wheat (McMechan and Hein 2017; Staples and Allington 1956). Thus, the most important tool available for management of this virus complex is the control of preharvest volunteer wheat that serves as an excellent bridge host (Wegulo et al. 2008).

If this green bridge is not broken before fall planting, there is a high risk that mites will move to the new wheat crop after it emerges and subsequently transmit the virus. Throughout the fall, mites continue to multiply and disperse from volunteer wheat, and the rate of virus transmission within adjoining fields increases. The risk for serious virus infection on winter wheat can be decreased by delayed planting dates in the fall (Hunger et al. 1992; McMechan and Hein 2016; Slykhuis et al. 1957; Staples and Allington 1956). Reduced risk with shortened exposure periods through the fall (i.e., later planting dates) also demonstrates that continuous mite movement and subsequent virus transmission increasingly impacts disease spread and severity. Alternately, spring infections result in much lower or often insignificant virus impact (Hunger et al. 1992; Staples and Allington 1956; Wosula et al. 2018). In the central Great Plains, virus symptom expression is minimal throughout the fall but rapidly increases in severity with the onset of warm temperatures (i.e., above 27°C) in the spring (Hunger 2010; Wegulo et al. 2008). However, warmer fall temperatures (e.g., during warmer falls or in more southern areas) are likely to accelerate symptom development.

WCMs disperse on the wind; therefore, the risk of mite movement and virus spread is dependent on the distance of the field from the mite source population. Staples and Allington (1956) and Workneh et al. (2009) sampled transects in a single direction away from a source and described disease gradients across fields adjacent to mite sources. Coutts et al. (2008), using transect sampling in two opposite directions, identified differences in mite movement gradients with greater mite movement in the prevailing wind direction. However, in the Great Plains wind direction changes regularly with the movement of weather fronts. The combination of regularly changing wind direction and mite movement continuing through the fall creates the potential for the extent of mite movement to change depending on the direction from a source field; however, the extent and pattern of this directional mite movement and virus spread have never been documented. To improve management of this virus complex, it is critical to understand the potential spatial spread of mite movement surrounding a mite-virus source field that accumulates through the fall, thus impacting the resulting virus epidemic risk.

Owing to the small size of WCMs, their movement is hard to quantify; however, the viruses they transmit produce symptoms that can be detected visually. WSMV interferes with chloroplast development of systemically infected wheat (Brakke et al. 1988; White and Brakke 1983), and infection causes a disruption of pigments, macromolecules, proteins, and nucleic acids in chloroplasts and a reduction of chlorophyll (Brakke et al. 1988). Initial symptoms of all WCM-vectored viruses are similar and include yellow to light green streaking, spotting, or mottling (De Wolf and Seifers 2008; Wegulo et al. 2008). In

†Corresponding author: G. L. Hein; E-mail: ghein1@unl.edu

Funding: This project was supported by the USDA National Institute of Food and Agriculture North Central Integrated Pest Management Grants Program, grant no. 2006-34103-16732.

Accepted for publication 15 August 2018.

Nebraska, virus symptoms do not appear until temperatures rise in April or May and rapidly become more intense to include stunting, rosetting, and extreme chlorosis (Wegulo et al. 2008).

Remotely sensed changes in wheat resulting from WSMV infection have been demonstrated. Workneh et al. (2009) used a handheld hyperspectral radiometer to determine virus infection severity and developed a model to predict yield impacts based on the extent of virus symptoms (Workneh et al. 2017). The potential for separating and classifying healthy and WSMV-infected wheat based on training samples from satellite-collected reflectance data was demonstrated by Mirik et al. (2011). Stilwell et al. (2013) used ground-based sensing to demonstrate that the red edge position (REP) vegetation index can be used effectively to detect WCM-vectored virus symptoms. These studies document the potential for using remote sensing to detect WCM-transmitted virus symptoms and to spatially quantify the cumulative effect of mite movement and subsequent virus spread in all directions from a mite source. However, it is important to recognize that these studies did not focus on separating reflectance characteristics from other potential stresses, and thus, they relied heavily on ground-based validation of virus presence (Bravo et al. 2003; Devadas et al. 2009; Mahlein 2016; Yuan et al. 2014).

A better understanding of the complete spatial pattern of mite movement and virus spread from a mite source will enhance our ability to identify the sphere of influence across the landscape around mite-virus source fields where risk of a virus epidemic is increased. Whole field studies addressing virus spread would be impractical because they would risk large areas of adjoining cropland; therefore, mite movement and virus spread into wheat were evaluated around small, mite-infested plots established within commercial wheat fields. The objectives of this study were to (i) establish a detailed spatial pattern of WCM movement and WSMV spread surrounding a central mite-virus source by using remote sensing to map the spatial occurrence of virus symptoms, (ii) determine the effects of wind speed and direction and mite density at the source on mite movement and virus spread, and (iii) use the data generated in these small-plot studies to make predictions of WSMV spread in wheat fields.

Materials and Methods

Study site. Stilwell et al. (2013) used proximal (ground-based) sensors to establish a correlation between the REP vegetation index and virus infection of wheat. The current study was conducted concurrently at the same sites and builds on the data reported by Stilwell et al. (2013), and many of the biophysical parameters on the ground were measured similarly for both studies. However, this study involved separate aerial-based hyperspectral remote sensing that enabled continuous spatial characterization of reflectance changes, and it also included more intensive ground-based sampling.

To simulate natural volunteer wheat conditions, wheat was established in two small plots (10 × 10 m) in the middle of a fallow wheat field (approximately 10 ha) at the University of Nebraska's High Plains Agricultural Laboratory near Sidney, Nebraska, on 13 July 2006 (41°14′06″N, 103°00′33″W), 12 July 2007 (41°14′16″N, 103°00′04″W), and 21 July 2008 (41°14′21″N, 102°59′57″W). The two plots, a north and a south plot, were separated by at least 120 m each year to avoid interference. Simulated volunteer wheat plots were infested with field-collected WCMs on 10 August 2006, 14 August 2007, and 26 August 2008 as described by Stilwell et al. (2013).

A weather station (CR10X datalogger, Campbell Scientific, Logan, UT) was placed in the middle of one volunteer source plot in September of each year, and data were collected hourly to monitor weather conditions during the fall mite movement period. Mean temperature, wind speed, and wind direction were determined between 27 September and 30 November of each year. This encompassed the period between wheat emergence and winter dormancy in western Nebraska, which is the period of primary concern for mite movement and virus spread. The proportion of hours when wind speeds were over 4.5 or over 9 m/s for each data set was calculated, and maximum wind speed and direction were determined.

A WSMV-susceptible wheat variety was planted surrounding the volunteer plots on 20 September 2006 (cv. Goodstreak; 9.5 ha), 8 September 2007 (cv. Millennium; 12.7 ha), and 16 September 2008 (cv. Overland; 8.8 ha). Biophysical sampling of this wheat was done at sampling points on concentric rings laid out at intervals of 7.6 m from the plot center around each plot (Fig. 1). Sampling points on these rings were located at each cardinal and ordinal direction from the plot as described by Stilwell et al. (2013). In the spring of each year when visual symptoms were apparent, additional sampling rings or partial rings were added between the primary rings to more completely encompass the spatial pattern of the symptom gradient (Fig. 1). The distance from the center of the source plot to the farthest sampling points extended well beyond the spatial spread of visible virus symptoms and varied between plots and years (2007 north, five rings out to 15.2 m; 2007 south, seven rings out to 22.9 m; 2008 north, seven rings out to 38.1 m; 2008 south, six rings out to 45.7 m; and 2009, eight rings out to 61.0 m). The density of sampling points varied depending on the spread of virus, with a higher density of sampling points located closer to the mite source plot when virus spread was more limited. This increased the ability to characterize the spatial relationship of symptom spread. Owing to a serious weed infestation present across much of one plot area, only one plot was utilized in 2008–09. This enabled much more intensive sampling of the remaining plot this year, and 128 additional sampling points were interspersed within the original sampling pattern. All sampling points in all years were georeferenced with submeter accuracy (Trimble TSCe, Tripod Data Systems).

Mite sampling. Plants within volunteer wheat (mite source) plots were sampled periodically (approximately 4 to 5 times) between mid-August and mid-November to determine mite population density. Twenty plants were randomly collected from each plot, and the number of mites per tiller was counted for all tillers of each plant in 2006 and for two randomly chosen tillers per plant in 2007 and 2008. Mean number of mites per tiller in source plots was calculated for each date. To measure mite movement from source plots into surrounding wheat that accumulated throughout the fall, sampling of wheat plants occurred late in the fall after the plants had entered dormancy and temperatures were well below those conducive for mite activity. Plant collections were made in 2006 (north, 5 December, n = 54; south, 16 November, n = 92), 2007 (north, 15 November, n = 76;

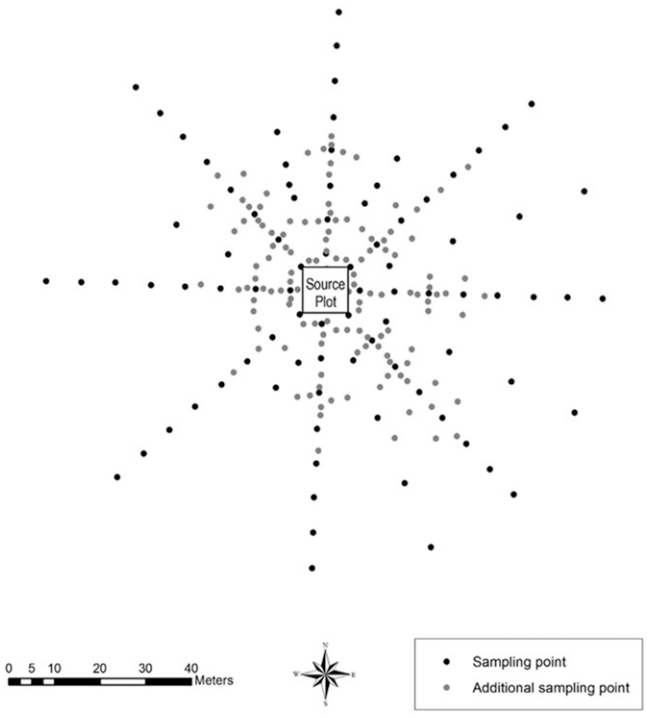

Fig. 1. Spatial layout of sampling pattern surrounding the mite-virus source plots. Location of the original sampling points (black) laid out in concentric rings with points on the cardinal and ordinal directions, and sampling points (gray) where additional relative chlorophyll and leaf area index measurements were taken.

south 5 December, $n = 76$), and 2008 (8 December, $n = 76$). Using a stereo microscope, mites were counted on three randomly selected tillers from each of 10 plants that had been randomly collected within an area of 0.5-m radius surrounding each sampling point.

Biophysical measurements. Measurements of relative chlorophyll, leaf area index (LAI), and virus incidence were taken during the heading stages of wheat when virus symptoms were near their peak. A Minolta SPAD-502 chlorophyll meter (Minolta Camera, Osaka, Japan) was used to provide a unitless measure of relative chlorophyll content. Chlorosis is highly associated with WCM-vectored viruses (Brakke et al. 1988; Wegulo et al. 2008), and the SPAD meter has proven to be an efficient tool for measuring chlorosis resulting from WSMV infection (Byamukama et al. 2014; Kariya et al. 1982; Yadava 1986).

Relative chlorophyll content was determined by averaging SPAD readings taken from 20 different flag leaves within a 1-m^2 area surrounding each sample point. Each reading was taken at approximately one-third the distance from the base to the tip of each flag leaf.

Because plant stunting and spraddling are symptoms of severe WSMV infection (Wegulo et al. 2008; Wosula et al. 2018), LAI was determined by using an LAI-2000 Plant Canopy Analyzer (Li-Cor, Lincoln, NE). For each LAI measurement, one above-canopy reading was taken, and four below-canopy readings were made along a diagonal transect between rows (30-cm row spacing).

In 2007, relative chlorophyll measurements were taken on 4 June, and the majority of LAI measurements were taken on 1 and 4 June (north, $n = 43$; south, $n = 67$); however, a few LAI measurements were delayed by approximately 1 week owing to unfavorable weather. In 2008, relative chlorophyll readings in both plots and LAI measurements in the south plot were acquired between 3 and 6 June (north, $n = 62$; south, $n = 70$). LAI readings taken in the north 2008 plot were delayed by approximately 2 weeks owing to unfavorable weather conditions. In 2009, relative chlorophyll readings were obtained between 18 and 19 June, and LAI readings were obtained between 8 and 15 June ($n = 216$). Wheat was in the flowering stage in 2007 and 2008 and late milk to early dough stage in 2009 when data were collected.

Following the collection of relative chlorophyll and LAI data, plant samples were collected to determine virus incidence. At each sampling point, 10 wheat tillers were randomly selected, bagged, returned to the laboratory, and frozen. Samples were collected on 8 June 2007 (north, $n = 43$; south, $n = 67$), between 4 and 6 June 2008 (north, $n = 62$; south, $n = 70$), and on 23 June 2009 ($n = 76$). WSMV infection in each of the 10 sampled tillers at each sample site was determined by using an enzyme-linked immunosorbent assay (ELISA) as described by Byamukama et al. (2013). Absorbance of each ELISA plate was read at 405 nm (MR 4000 Micro ELISA plate reader; Dynatech Laboratories, Chantilly, VA). Plants were considered positive for WSMV when the mean absorbance of the replicate samples was greater than two times the mean absorbance of negative controls in the sample plate. The percentage of infected tillers at each sampling point was determined.

Hyperspectral measurements. Hyperspectral images were collected on 8 June 2007, 30 May 2008, and 22 June 2009. All images were collected between 0830 and 1200 CST. Hyperspectral images were acquired with an airborne AISA-Eagle hyperspectral sensor (Spectral Imaging, Oulu, Finland) by the Center for Advanced Land Management Information Technologies (University of Nebraska–Lincoln). Images were collected with a single flight line with ground speed of 220 km/h at an altitude of 1,158 m above ground level (39.7° field of view). The AISA-Eagle collected spectral data between 400 and 970 nm. The spectral resolution was 2.9 nm, and the slit width was 30 μm. Images were acquired at 1.0-m spatial resolution, corrected for atmospheric effects with the Fast Line-of-Sight Atmospheric Analysis of Spectral Hypercubes (FLAASH) software, and georectified with ENVI image analysis software by using ground control points (ESRI 2006; Matthew et al. 2003; Narumalani et al. 2009). Georectification was performed by using the first-order polynomial method and resampled using the nearest neighbor approach.

Data analysis. Stilwell et al. (2013) identified the REP vegetative index as the best of several indices to identify WSMV symptoms in wheat. REP (Guyot and Baret 1988) was calculated for each pixel of each image by using the following equations:

$$\mathrm{REP} = 700 + 40\frac{\rho_{\mathrm{rededge}} - \rho_{700\mathrm{nm}}}{\rho_{740\mathrm{nm}} - \rho_{700\mathrm{nm}}}$$

$$\rho_{\mathrm{rededge}} = \frac{\rho_{670\mathrm{nm}} + \rho_{780\mathrm{nm}}}{2}$$

where ρ_x is the reflectance value at wavelength x.

Georeferenced sampling locations used for biophysical measurements were located on the image, and REP values were recorded for each sampling point. Pearson correlation coefficients among the biophysical variables and REP were calculated for each data set (SAS Institute 2002, PROC CORR).

It was possible to establish biophysical parameters at only a limited number of sites as described above, but remote sensing imagery can provide continuous data across a landscape at 1-m resolution. This imagery and its correlation with the ground-based biophysical variables enable spatial interpolation based on the assumption that objects that are close together tend to have greater correlation. Cokriging is an interpolation method that calculates predictions for the undersampled (primary) variable with the help of the oversampled (secondary) variable to improve the accuracy of predicting values at unsampled sites (Estrada-Peña 1999; Mutanga and Rugege 2006; Tarr et al. 2005; Van der Meer 1998). It utilizes a linear model of coregionalization that makes use of both the spatial autocorrelation in the primary variable and the cross-correlation between the primary and secondary variables (Hudak et al. 2002). In remote sensing studies, the primary variable generally originates from field observations, whereas the secondary variable is derived from remote sensing imagery (Van der Meer 1998). Cokriging uses the semivariance to express the degree of relationship between points. The semivariance is the average of the squared differences between all possible points spaced a constant distance apart. When data are spatially correlated, the semivariance increases as points are compared with increasingly distant locations.

Cokriging was applied with the Geospatial Analyst in ArcMap 9.2 (ESRI 2006) to develop a prediction map for each data set. To fit the model, field observations were used for the primary variable, and remote sensing imagery was used for the secondary variable. To determine if each of the variables exhibited a normal distribution, the histogram and normal QQPlot, which compares the distribution of the data to a standard normal distribution, were examined for each of the data sets. A spherical model with a nugget component was fit to the semivariogram. Lag size multiplied by the number of lags was less than half the largest distance in the dataset (<61.3 m). The partial sill and nugget values were set to default values because these were already the optimal values.

We hypothesized that WCM movement and virus symptoms were directionally dependent and would display anisotropy in the cokriging model because mites disperse via wind. Geostatistical Analyst was used to automatically calculate the optimal parameters to account for anisotropic influence. Each model was checked for anisotropy, and the direction of anisotropy associated with each model was determined.

Leave-one-out cross-validation was used to determine the accuracy of each model. In this cross-validation method, each point in the sampling scheme was removed individually, and its value was predicted by cokriging the remaining data (Tarr et al. 2005). The coefficients of determination (R^2) for the cross-validation between each biophysical variable and REP were calculated by regressing the values predicted by cokriging onto the measured values for each model in each data set (SAS Institute 2002, PROC REG), and a P of 0.05 was used to determine significance.

Results

Study site. Average hourly wind direction and the percentage of the total hours recorded at various wind speeds for each year and plot

are listed in Table 1. The maximum wind speed was 14.9 m/s in 2006, 15.7 m/s in 2007, and 17.8 m/s in 2008. The mean daily temperature between 27 September and 30 November was 6.3°C in 2006, 7.8°C in 2007, and 7.6°C in 2008. The mean number of mites per tiller in the WCM source volunteer plots varied between years and between plots (Table 2). The highest mite populations occurred in 2008–09 (17 October) followed by the 2006–07 south (12 October) and the 2007–08 north (11 October) plots.

Biophysical measurements. *2006–07.* Spread of WCMs and subsequent virus infection extended in all directions from the WCM source plots (north and south) in the spring, but spread was limited to a few meters. Even with limited spread, virus symptoms were more visible south and east of the plots. The mite density in source plots after wheat emerged was 41.4 mites per tiller in the north plot and 135.0 in the south plot (Table 2); however, a limited number of sampling points were encompassed by virus spread, and we were unable to statistically describe the spatial pattern of symptoms.

Correlation coefficients between REP and the biophysical variables in the 2006–07 data sets were not statistically significant. A cokriging model could not be fit to any variable for either of the 2006–07 data sets, indicating no measurable spatial pattern. The 2006–07 data were not used in further analysis.

2007–08. A discernible pattern of virus symptoms with a severity gradient extending in all directions was visible around the mite source plots. Although mild chlorosis was noticeable in tillers located further from the source plots, the majority of yellowing was observed within 15 m of the source plot. Stunted plants were common close to source plots, with severity decreasing with distance. Chlorosis and stunting formed an obvious oval pattern surrounding the source plots, and this oval was displaced to the southeast. Chlorosis was more visible in the north plot than in the south plot.

The mean number of mites per tiller, the percentage of tillers infested in the fall of 2007, and the mean percentage of tillers infected with WSMV in the spring of 2008 were highest near the WCM source plots in each data set and decreased with distance. Mite density in the source plots following wheat emergence varied considerably, from 98.8 mites per tiller in the north plot down to 27.6 mites per tiller in the south plot (Table 2). Relative chlorophyll readings generally were in the 40s for healthy plants, whereas plants with severe virus symptoms generally had readings near or below 30. Individual SPAD readings ranged from 25 to 48.2 in the north plot and 28.2 to 47.9 in the south plot. LAI values ranged from 0.97 to 4.07 in the north plot and 1.7 to 3.9 in the south plot. LAI was significantly correlated with relative chlorophyll in the south plot but did not have a significant relationship with any of the other biophysical variables (Table 3). This can be attributed to the limited range of LAI values. Significant correlation coefficients among the biophysical variables ranged from 0.37 to 0.82 in the north plot and from 0.34 to 0.84 in the south plot (Table 3).

2008–09. Significant virus symptoms were observed surrounding the source plot. Plants closest to the source plot were severely chlorotic, and chlorosis continued to be visible approximately 30 to 38 m from the source plot. Symptoms appeared to be distributed in an oval pattern surrounding the source plots that was displaced to the southeast.

Mean values for biophysical parameters associated with mite movement (mean mites per tiller and percentage of tillers infested) in the fall of 2008 and virus symptoms in the spring of 2009 (percentage of tillers infected with WSMV, relative chlorophyll, and LAI) decreased with distance from the WCM source plot. Mite density in the fall following wheat emergence was the highest of any plots and averaged 232.2 mites per tiller (Table 2). Individual SPAD readings ranged from 10.6 to 44.7, and LAI values ranged from 0.72 to 4.16. Correlation coefficients among the biophysical variables were much higher than in 2007–08 and ranged from 0.49 to 0.84 (Table 3).

Hyperspectral measurements. All of the biophysical variables for each plot were significantly correlated to REP (Table 3). Relative chlorophyll values and LAI increased with increasing REP values; however, mites per tiller, percentage of tillers infested with mites, and percentage of tillers infected with virus decreased with increasing REP. The lowest correlation coefficients for REP occurred in the 2007–08 south plot (range: 0.37 to 0.84), which also had the lowest symptom severity.

Cokriging. REP was spatially correlated with percentage of virus infection and relative chlorophyll values in all three plots according to the semivariance. REP was spatially correlated with LAI and percentage of tillers infested with mites in the 2007–08 north and 2008–09 plots. Because these variables were spatially correlated, it was possible to fit a model between REP and these variables by using cokriging.

The coefficients of determination (R^2) for the cross-validation between each biophysical variable and the REP vegetation index were higher for percentage of virus infection than for relative chlorophyll values for the 2007–08 plots (Table 4). The R^2 was higher for relative chlorophyll values (R^2 = 0.82) than percentage of virus infection (R^2 = 0.74) in the 2008–09 plot. Because of the importance in determining the extent of WCM movement and subsequent WSMV spread from the source plots, percentage of virus infection was determined to be the most useful primary variable to utilize in the cokriging model. By using percentage of virus infection as the primary variable in cokriging, a prediction map was created that displayed the spatial pattern associated with specific classes of virus infection.

Table 1. Average hourly wind direction and percentage of hours at various wind speeds during the fall mite movement period (27 September to 30 November) and degree of anisotropy associated with each cokriging model

	Mean hourly wind direction (percentage of hours at specified wind speed)			
Year	Wind speed >0 m/s (0 to 17.8 m/s)	Wind speed ≥4.5 m/s (4.5 to 17.8 m/s)	Wind speed ≥9 m/s (9.0 to 17.8 m/s)	Degree of anisotropy
2006–07	231.1° (100%)	261.4° (30.5%)	313.0° (1.9%)	–
2007–08	260.6° (100%)	290.0° (33.8%)	323.5° (4.4%)	North: 333.7° South: 334.2°
2008–09	237.7° (100%)	270.1° (33.5%)	312.0° (6.8%)	319.2°

Table 2. Mean number of wheat curl mites per wheat tiller in source volunteer plots through the fall (mean ± SE)

	Number of wheat curl mites per tiller in mite source plots				
Date	2006–07 north	2006–07 south	2007–08 north	2007–08 south	2008–09
Date 1	73.1 ± 10.5 (24 Aug)	19.8 ± 3.1 (24 Aug)	10.6 ± 2.8 (16 Aug)	4.4 ± 1.4 (16 Aug)	–
Date 2	–	–	22.5 ± 3.7 (30 Aug)	10.8 ± 2.1 (30 Aug)	26.3 ± 5.7 (3 Sept)
Date 3	24.4 ± 2.9 (8 Sept)	–	82.6 ± 8.8 (14 Sept)	74.3 ± 12.5 (14 Sept)	76.2 ± 11.5 (16 Sept)
Date 4[a]	23.6 ± 2.2 (27 Sept)	48.1 ± 6.0 (27 Sept)	92.1 ± 20.6 (26 Sept)	30.0 ± 6.8 (26 Sept)	149.0 ± 18.4 (30 Sept)
Date 5	59.2 ± 10.3 (12 Oct)	221.9 ± 27.8 (12 Oct)	105.4 ± 21.3 (11 Oct)	25.3 ± 4.3 (11 Oct)	315.4 ± 31.8 (17 Oct)

[a] Wheat surrounding the mite source plot had emerged prior to mite sampling on date 4.

The geographic information system utilized to perform cokriging allowed up to three secondary variables to be utilized. Therefore, cokriging was used to determine if R^2 could be increased by utilizing percentage of virus infection as the primary variable and both the REP index and relative chlorophyll readings as secondary variables. The addition of relative chlorophyll values as a secondary variable did not greatly affect R^2 in the 2007–08 data (north, $R^2 = 0.56$; south, $R^2 = 0.43$) because relative chlorophyll values were not oversampled compared with percentage of virus infection that year. However, R^2 increased from 0.74 to 0.78 and the root mean square error was reduced by 7.8% (from 17.28 to 15.93) by adding relative chlorophyll values as a secondary variable in 2008–09. The additional sampling locations where only relative chlorophyll values were measured in 2008–09 may have effectively resulted in an increased R^2 for the model between percentage of virus infection and REP index. In 2007–08, the same number of samples were collected for virus infection determination and relative chlorophyll. To remain consistent when developing models across data sets, cokriging models were developed for each data set by utilizing percentage of virus infection as the primary variable and the REP index and relative chlorophyll values as the secondary variables.

The histogram and normal QQPlot were normally distributed for each of the three data sets. Lag size and lag number were 6.4 and 12 (2007–08 north plot), 7.7 and 10 (2007–08 south plot), and 7.4 and 12 (2008–09 plot), respectively. The partial sill and nugget default values were 699.0 and 202.2 for the 2007–08 north plot, 548.7, and 291.0 for the 2007–08 south plot, and 1,284.5 and 57.1 for the 2008–09 plot, respectively. The major range resulting from anisotropic effects in the data sets was 48.3 for the 2007–08 north plot, 75.9 for the 2007–08 south plot, and 62.5 for the 2008–09 plot. The direction of anisotropy was similar for all three data sets (Table 1).

The predicted variables determined by cokriging were classified into four classes based on virus incidence (0 to 25, 25 to 50, 50 to 75, and 75 to 100%). The spatial patterns of virus spread predicted by cokriging are displayed for each data set (Fig. 2). In each map, cokriging predicted the highest percentage of virus infection to be closest to the plots, with virus incidence decreasing with distance from the source plot. The maps displayed a generally oval-shaped pattern of virus spread that was displaced to the southeast for each data set. These observations were consistent with the degree of anisotropy in the associated models as well as visible virus symptoms observed in the field.

Discussion

The REP indices calculated from the airborne hyperspectral sensor data were found to be effective in evaluating WSMV spread. The REP indices correlated with biophysical variables associated with symptoms of WCM-vectored viruses, and these data enabled the production of cokriged prediction maps of the spatial pattern of virus spread surrounding a central mite-virus source. The reflectance relationships with biophysical variables calculated in this aerial-based study were comparable but slightly lower than previous relationships from proximal data from Stilwell et al. (2013). However, aerial data provided continuous 1-m spatial resolution across the dispersal plots. Small differences between proximal and aerial reflectance data may be attributed to atmospheric effects on aerial data, resulting in a relatively uniform reduction in reflectance across the visible spectrum and more effective absorption as well as scattering in the near-infrared region.

The detailed resolution from the airborne sensors enabled quantification of the spatial structure of mite movement and virus spread surrounding a central mite-virus source. There have been reports on WSMV symptom gradients, but these studies have been limited to transects extending in a single or at most two directions from the source (Coutts et al. 2008; Workneh et al. 2009). Because we evaluated virus spread in the spring after symptoms were at their peak, the distribution of symptoms represents the spread of virus for the season. Previous work has indicated that virus infection

Table 4. Coefficients of determination (R^2) for the cross-validation between each biophysical variable and the red edge position vegetation index ($P < 0.001$)

	Coefficients of determination (R^2)		
Biophysical variable	**2007–08 north**	**2007–08 south**	**2008–09**
% virus infection	0.56 (n = 61)	0.42 (n = 70)	0.74 (n = 74)
Chlorophyll	0.37 (n = 61)	0.30 (n = 70)	0.82 (n = 215)
Leaf area index	0.66 (n = 62)	–[a]	0.76 (n = 211)
% tillers infested	0.22 (n = 43)	–[a]	0.71 (n = 76)

[a] Variable could not be modeled with cokriging owing to lack of spatial correlation.

Table 3. Degree of association (correlation coefficient, r) between biophysical variables, the red edge position (REP) vegetation index, and distance from the center of the mite source plot for each data set ($P < 0.05$)[a]

	Correlation coefficient (r)					
Site	**REP**	**RC**	**LAI**	**% virus infection**	**Mites per tiller**	**% tillers infested**
2007–08 north						
RC	0.80 (n = 61)	–				
LAI	0.76 (n = 62)	0.60[b] (n = 62)	–			
% virus infection	–0.71 (n = 61)	–0.69[b] (n = 61)	–0.59[b] (n = 61)	–		
Mites per tiller	–0.50 (n = 43)	–0.42 (n = 42)	NS	0.45 (n = 41)	–	
% tillers infested	–0.82 (n = 43)	–0.62 (n = 43)	–0.55 (n = 43)	0.70 (n = 43)	0.82 (n = 41)	–
Distance	0.67 (n = 63)	0.49 (n = 61)	0.61 (n = 62)	–0.68 (n = 61)	–0.37 (n = 43)	–0.62 (n = 43)
2007–08 south						
RC	0.84 (n = 70)	–				
LAI	0.37 (n = 70)	0.34[b] (n = 70)	–			
% virus infection	–0.58 (n = 70)	–0.56[b] (n = 70)	NS[b]	–		
Mites per tiller	–0.69 (n = 52)	–0.64 (n = 52)	NS	0.56 (n = 52)	–	
% tillers infested	–0.76 (n = 53)	–0.72 (n = 53)	NS	0.69 (n = 53)	0.80 (n = 52)	–
Distance	0.37 (n = 70)	0.45 (n = 70)	NS	–0.56 (n = 70)	–0.36 (n = 52)	–0.59 (n = 53)
2009-09						
RC	0.79 (n = 215)	–				
LAI	0.81 (n = 211)	0.66 (n = 210)	–			
% virus infection	–0.72 (n = 74)	–0.82 (n = 74)	–0.71 (n = 73)	–		
Mites per tiller	–0.49 (n = 76)	–0.64 (n = 76)	–0.51 (n = 76)	0.60 (n = 74)	–	
% tillers infested	–0.72 (n = 76)	–0.84 (n = 76)	–0.70 (n = 75)	0.82 (n = 74)	0.83 (n = 76)	–
Distance	0.73 (n = 76)	0.82 (n = 76)	0.69 (n = 75)	–0.77 (n = 74)	–0.50 (n = 76)	–0.71 (n = 76)

[a] RC = relative chlorophyll; LAI = leaf area index; and NS = not significant.
[b] From Stilwell et al. (2013).

originating in the fall before winter dormancy has the greatest impact on wheat (Hunger et al. 1992; Wosula et al. 2018). In all plots, the cumulative virus spread indicated that mites moved the virus to some degree in all directions. This would be expected from varying wind directions occurring through the fall mite movement period.

Even though virus spread was seen to occur in all directions, both visible symptoms in the field and predictions by cokriging showed virus symptoms extended further to the southeast of the source plots. The degree of anisotropy for the cokriged plots was approximately from the northwest (319 to 334°; Table 1). However, mean hourly wind direction was from the west to southwest (231 to 261°) during the fall mite movement period (Table 1). Predominant winds in the region come from both the northwest and south/southeast; therefore, it is logical that the average wind direction would be between these two directions (i.e., southwest). The average direction of winds over 9 m/s during the fall ranged from 312° to 323°, and this was close to the degree of anisotropy seen in the cokriged plots, 319° to 334° (Table 1). In addition, the percentage of hours with wind speeds greater than 9 m/s was highest for the plots with greatest dispersal (2008–09) and much lower for the plots where dispersal was limited (2006–07; Table 1). This pattern of virus spread that is more prevalent in the direction of the highest wind speeds indicates that WCMs disperse more readily when wind speeds are higher. In the central high plains of the United States, strong northwesterly winds are associated with high-pressure systems (i.e., increased barometric pressure) and more clear weather conditions. These conditions would be more favorable for mites to move and establish on new hosts. An association between dispersal and rising barometric pressure has been demonstrated for twospotted spider mites (Li and Margolies 1994) and could be a factor in WCM dispersal.

Mite dispersal in the fall is not visually apparent, and expression of symptoms caused by virus transmission in the fall is generally delayed until temperatures rise in the spring (Wegulo et al. 2008; Wosula et al. 2017). Even though primary mite infestation in the fall was not clear visually, mite infestation (percentage of infested tillers) correlated with most virus-associated symptoms (i.e., relative chlorophyll, LAI, and percentage of virus infection) in the spring (Table 3). However, mites per tiller was not spatially correlated with REP for any plot. This was likely owing to high variability involved in sampling mites, and greater sampling effort would be needed to better evaluate this relationship. However, percentage of tillers infested with mites was spatially correlated with REP for some plots (Table 4). When virus spread outside the mite source plot was greatest (2008–09), the relationship between percentage of tillers infested with mites and REP was comparable to the other three biophysical variables, even though percentage of tillers infested with mites was not sampled as intensively as with relative chlorophyll and LAI (Table 4).Thomas and Hein (2003) indicated that WCM movement and subsequent WSMV spread were dependent on the mite density of the source. In the current study, densities of WCMs in the source plots were significantly different between plots (Table 2), and the highest mite density coincided with the greatest virus spread (2008–09). However, this was not always the case, because mite dispersal was considerably limited in 2006–07, even with moderate mite densities. These results demonstrate that other factors are also important.

Lower velocity winds occurring in 2006–07 were noted earlier, but one additional factor that may have limited spread was lower fall temperatures. The mean daily fall temperature was lowest in 2006 compared with 2007 and 2008. Temperature is an important factor that influences the abundance and activity of virus vectors and viruses in plants (Thresh 1976) and WSMV specifically (Wosula et al. 2017). Cooler temperatures during fall months of this study may have limited WCM movement and subsequent virus development in 2006–07. Thus, the spatial relationship of mite movement and virus spread likely is influenced by multiple important factors, including wind direction and speed, mite density at the source, and fall temperatures. Accurate predictions of spread must account for these factors.

Prediction of the sphere of influence that establishes virus risk surrounding a mite-virus source is critical to optimal management of this virus complex. Full-field-scale experiments involving the release of virus-infected mites would be difficult and impractical owing to potential impacts on wheat in the surrounding agroecosystem. However, the results of this small-plot study were utilized to estimate the potential spatial spread of WCMs and subsequent virus spread at the whole-field scale. For example, if the small mite-virus source plots (10 × 10 m) used in this study were increased to 32.4 ha (80 acres; 569 × 569 m) and the source population of WCMs and weather conditions were similar to those in 2008–09, we can estimate the distance of spread using Figure 2. Using comparative ratios ($10/x = 569/y$, where x is the distance value estimate from Figure 2 and y is the estimated distance of spread at the larger scale), we can predict the spatial spread of mites and virus.

Assuming WCM movement under these conditions would progress in a linear fashion as the mite-virus source increases in size, movement in the southeast direction would potentially result in the following: 75 to 100% of tillers infected 1.4 km from the center of the source field, 50 to 75% of tillers infected 2.2 km from the center of the source field, and 25 to 50% of tillers infected 3.3 km from the center of the source field. The validity of the assumption that a linear increase with increasing scale for this relationship would occur is difficult to establish. However, mite movement is extremely difficult to measure, and this provides an estimate of potential distance and spatial structure of virus spread from a central mite-virus source. Based on numerous observations made during epidemic occurrences in the field, these estimates appear reasonable; however, future efforts to track virus presence on a larger scale may enable validation of these virus spread estimates in naturally occurring epidemic situations.

It is clear from this study that the sphere of influence (virus infection risk) surrounding a mite-virus source field extends in all

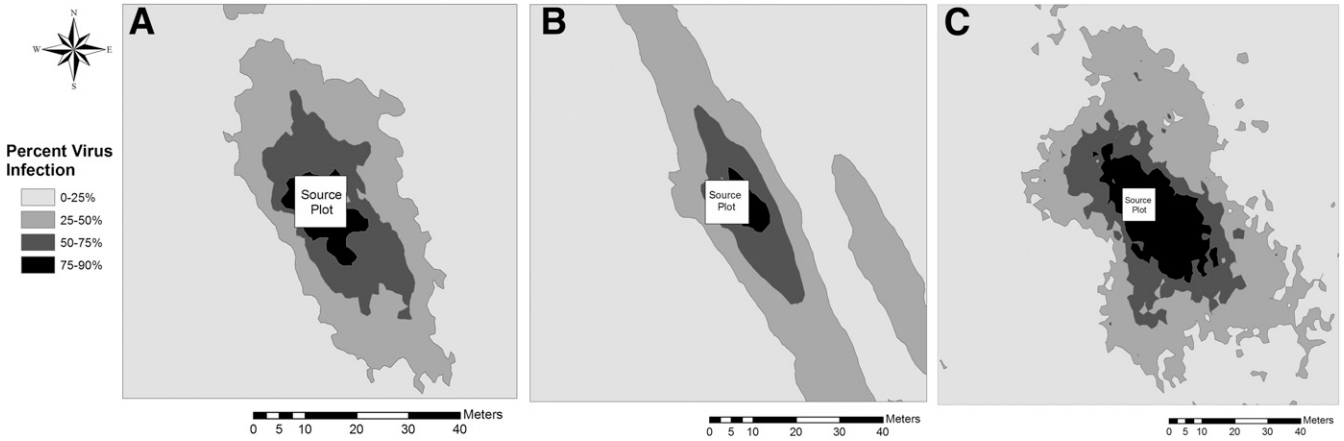

Fig. 2. Spatial spread of different infection classes surrounding each of the wheat curl mite source plots as predicted by cokriging: **A,** 2007–08 north; **B,** 2007–08 south; and **C,** 2008–09.

directions, but it extends further in the direction of the highest winds. Risk parameters established from these distance estimates could be used by wheat growers to evaluate and predict the potential sphere of influence for mite source fields (e.g., volunteer wheat). This information can be used to improve management decisions, such as prioritizing control of preharvest volunteer wheat or use of virus-resistant wheat varieties in areas of highest risk.

Acknowledgments

The airborne AISA-Eagle sensor system is owned and operated by the Center for Advanced Land Management Information Technologies (CALMIT), School of Natural Resources, University of Nebraska–Lincoln. We thank Richard Perk, CALMIT, for his considerable assistance and Susan Harvey, Rick Patrick, and John Thomas for their technical assistance and support.

Literature Cited

Brakke, M. K., White, J. L., Samson, R. G., and Joshi, J. 1988. Effect of wheat streak mosaic virus infection on total DNA and chloroplast ribosomal RNA in wheat leaves. J. Phytopathol. 123:156-164.

Bravo, C., Moshou, D., West, J., McCartney, A., and Ramon, H. 2003. Early disease detection in wheat fields using spectral reflectance. Biosyst. Eng. 84: 137-145.

Burrows, M., Franc, G., Rush, C., Blunt, T., Ito, D., Kinzer, K., Olson, J., O'Mara, J., Price, J., Tande, C., Ziems, A., and Stack, J. 2009. Occurrence of viruses in wheat in the Great Plains region, 2008. Online publication. Plant Health Prog. 10.

Byamukama, E., Seifers, D. L., Hein, G. L., De Wolf, E., Tisserat, N. A., Langham, M. A. C., Osborne, L. E., Timmerman, A., and Wegulo, S. N. 2013. Occurrence and distribution of Triticum mosaic virus in the Central Great Plains. Plant Dis. 97:21-29.

Byamukama, E., Wegulo, S. N., Tatineni, S., Hein, G. L., Graybosch, R. A., Baneziger, P. S., and French, R. 2014. Quantification of yield loss caused by Triticum mosaic virus and wheat streak mosaic virus in winter wheat under field conditions. Plant Dis. 98:127-133.

Connin, R. V. 1956. Oversummering volunteer wheat in the epidemiology of wheat streak-mosaic. J. Econ. Entomol. 49:405-406.

Coutts, B. A., Strickland, G. R., Kehoe, M. A., Severtson, D. L., and Jones, R. A. C. 2008. The epidemiology of wheat streak mosaic virus in Australia: Case histories, gradients, mite vectors, and alternative hosts. Aust. J. Agric. Res. 59:844-853.

Devadas, R., Lamb, D. W., Simpfendorfer, S., and Backhouse, D. 2009. Evaluating ten spectral vegetation indices for identifying rust infection in individual wheat leaves. Precis. Agric. 10:459-470.

De Wolf, E., and Seifers, D. 2008. Triticum Mosaic: A New Wheat Disease in Kansas. Publication EP-145. Kansas State University, Manhattan.

Environmental Systems Resource Institute (ESRI). 2006. ArcMap 9.2. ESRI, Redlands, CA.

Estrada-Peña, A. 1999. Geostatistics and remote sensing using NOAA-AVHRR satellite imagery as predictive tools in tick distribution and habitat suitability estimations for *Boophilus microplus* (Acari: Ixodidae) in South America. Vet. Parasitol. 81:73-82.

Guyot, G., and Baret, F. 1988. Utilisation de la haute resolution spectrale pour suivre l'etat des couverts vegetaux. Pages 279-286 in: 4th International Colloquium on Spectral Signatures of Objects in Remote Sensing, T. D. Guyenne and J. J. Hunt, eds. European Space Agency, SP-287, Aussois, France.

Hudak, A. T., Lefsky, M. A., Cohen, W. B., and Berterretche, M. 2002. Integration of lidar and Landsat ETM+ data for estimating and mapping forest canopy height. Remote Sens. Environ. 82:397-416.

Hunger, R. M. 2010. Wheat streak mosaic virus. Pages 115-117 in: Compendium of Wheat Diseases and Pests, 3rd Ed. W. W. Bockus, R. L. Bowden, R. M. Hunger, W. L. Morrill, T. D. Murray, and R. W. Smiley, eds. APS Press, St. Paul, MN.

Hunger, R. M., Sherwood, J. L., Evans, C. K., and Montana, J. R. 1992. Effects of planting date and inoculation date on severity of wheat streak mosaic in hard red winter wheat cultivars. Plant Dis. 76:1056-1060.

Kariya, K., Matsuzaki, A., and Machida, H. 1982. Distribution of chlorophyll content in leaf blade of rice plant. Jpn. J. Crop. Sci. 51:134-135.

Li, J., and Margolies, D. C. 1994. Barometric pressure influences initiation of aerial dispersal in the twospotted spider mite. J. Kansas Ent. Soc. 67:386-393.

Mahlein, A. K. 2016. Plant disease detection by imaging sensors—Parallels and specific demands for precision agriculture and plant phenotyping. Plant Dis. 100:241-251.

Matthew, M. W., Adler-Golden, A. M., Berk, A., Felde, G., Anderson, G. P., Gorodestzky, D., Paswaters, S., and Shippert, M. 2003. Atmospheric correction of spectral imagery: Evaluation of the FLAASH algorithm with AVIRIS data. Pages 474-482 in Proceedings of the SPIE Algorithms and Technologies for Multispectral, Hyperspectral, and Ultraspectral Imagery IX. Vol. 5093.

McMechan, A. J., and Hein, G. L. 2016. Planting date and variety selection for management of viruses transmitted by the wheat curl mite (Acari: Eriophyidae). J. Econ. Entomol. 109:70-77.

McMechan, A. J., and Hein, G. L. 2017. Population dynamics of the wheat curl mite (Acari: Eriophyidae) during the heading stages of winter wheat. J. Econ. Entomol. 110:355-361.

Mirik, M., Jones, D. C., Price, J. A., Workneh, F., Ansley, R. J., and Rush, C. M. 2011. Satellite remote sensing of wheat infected by wheat streak mosaic virus. Plant Dis. 95:4-12.

Mutanga, O., and Rugege, D. 2006. Integrating remote sensing and spatial statistics to model herbaceous biomass distribution in a tropical savanna. Int. J. Remote Sens. 27:3499-3514.

Narumalani, S., Mishra, D. R., Wilson, R., Reece, P., and Kohler, A. 2009. Detecting and mapping four invasive species along the floodplain of North Platte River, Nebraska. Weed Technol. 23:99-107.

Oldfield, G. N. 1970. Mite transmission of plant viruses. Annu. Rev. Entomol. 15: 343-380.

SAS Institute. 2002. PROC User's Manual, 6th Ed. SAS Institute, Cary, NC.

Seifers, D. L., Harvey, T. L., Martin, T. J., and Jensen, S. G. 1997. Identification of the wheat curl mite as the vector of the High Plains virus of corn and wheat. Plant Dis. 81:1161-1166.

Seifers, D. L., Martin, T. J., Harvey, T. L., Fellers, J. P., Stack, J. P., Ryba-White, M., Haber, S., Krokhin, O., Spicer, V., Lovat, N., Yamchik, A., and Standing, K. G. 2008. Triticum mosaic virus: A new virus isolated from wheat in Kansas. Plant Dis. 92:808-817.

Slykhuis, J. T., Andrews, J. E., and Pittman, U. J. 1957. Relation of date of seeding winter wheat in southern Alberta to losses from wheat streak mosaic, root rot, and rust. Can. J. Plant Sci. 37:113-127.

Staples, R., and Allington, W. B. 1956. Streak Mosaic of Wheat in Nebraska and Its Control. Agricultural Experiment Station, Research Bulletin 178. University of Nebraska, Lincoln.

Stilwell, A. R., Hein, G. L., Zygielbaum, A. I., and Rundquist, D. C. 2013. Proximal sensing to detect symptoms associated with wheat curl mite-vectored viruses. Int. J. Remote Sens. 34:4951-4966.

Tarr, A. B., Moore, K. J., and Dixon, P. M. 2005. Spectral reflectance as a covariate for estimating pasture productivity and composition. Crop Sci. 45:996-1003.

Thomas, J. A., and Hein, G. L. 2003. Influence of volunteer wheat plant condition on movement of the wheat curl mite, *Aceria tosichella*, in winter wheat. Exp. Appl. Acarol. 31:253-268.

Thresh, J. M. 1976. Gradients of plant virus diseases. Ann. Appl. Biol. 82:381-406.

Van der Meer, F. 1998. Mapping dolomitization through a co-regionalization of simulated field and image-derived reflectance spectra: A proof-of-concept study. Int. J. Remote Sens. 19:1615-1620.

Wegulo, S. N., Hein, G. L., Klein, R. N., and French, R. C. 2008. Managing Wheat Streak Mosaic. EC1871. University of Nebraska–Lincoln Extension.

White, J. L., and Brakke, M. K. 1983. Protein changes in wheat infected with wheat streak mosaic virus and in barley infected with barley stripe mosaic virus. Physiol. Plant Pathol. 22:87-100.

Workneh, F., Jones, D. C., and Rush, C. M. 2009. Quantifying wheat yield across the field as a function of wheat streak mosaic intensity: A state space approach. Phytopathology 99:432-440.

Workneh, F., O'Shaughnessy, S., Evett, S., and Rush, C. M. 2017. Relationships between early wheat streak mosaic severity levels and grain yield: Implications for management decisions. Plant Dis. 101:1621-1626.

Wosula, E. N., McMechan, A. J., and Hein, G. L. 2015. The effect of temperature, relative humidity, and virus infection status on off-host survival of the wheat curl mite (Acari: Eriophyidae). J. Econ. Entomol. 108:1545-1552.

Wosula, E. N., McMechan, A. J., Knoell, E., Tatineni, S., Wegulo, S. N., and Hein, G. L. 2018. Impact of timing and method of virus inoculation on the severity of wheat steak mosaic disease. Plant Dis. 102:645-650.

Wosula, E. N., Tatineni, S., Wegulo, S. N., and Hein, G. L. 2017. Effect of temperature on wheat streak mosaic disease development in winter wheat. Plant Dis. 101:324-330.

Yadava, U. L. 1986. A rapid and nondestructive method to determine chlorophyll in intact leaves. HortScience 21:1449-1450.

Yuan, L., Huang, Y., Loraamm, R. W., Nie, C., Wang, J., and Zhang, J. 2014. Spectral analysis of winter wheat leaves for detection and differentiation of diseases and insects. Field Crops Res. 156:199-207.